

A simulation study to estimate optimum LOR angular acceptance for the image reconstruction with the Total-Body J-PET

Meysam Dadgar^{1,2}, Szymon Parzych^{1,2}, and Faranak Tayefi Ardebili^{1,2}

¹ Marian Smoluchowski Institute of Physics, Jagiellonian University, Poland

² Total-Body Jagiellonian-PET Laboratory, Jagiellonian University, Poland

Abstract. One of the directions in today's development of PET scanners is to increase their axial field of view (AFOV). Currently limited to several centimeters, AFOV of the clinically available PET tomographs results in a very low sensitivity ($\sim 1\%$) and requires an extended time for a scan of a whole human body. While these drawbacks are addressed in the so-called, Total Body PET concept (scanner with a significantly elongated field of view), it creates new challenges not only in the mechanical construction but also in the image reconstruction and event selection. The possibility of taking into account of large angle variety of lines of responses (LORs) contributes positively to the sensitivity of the tomograph. However, at the same time, the most oblique LORs have an unfavorable influence on the spatial resolution due to the parallax error and large contribution to the scatter fraction. This forces to determine a new factor - acceptance angle - which is a maximum azimuthal angle for which the LORs are still taken into image reconstruction. Correct determination of such factor is imperative to maximize the performance of a Total Body PET system since it introduces a trade-off between the two main characteristics of scanners: sensitivity and spatial resolution. This work has been dedicated to the estimation of the optimal acceptance angle for the proposed by the Jagiellonian PET (J-PET) Collaboration Total Body tomograph. J-PET Collaboration introduces a novel, cost-effective approach to PET systems development with the use of organic scintillators. This simulation study provides evidence that the 45° acceptance angle cut can be an appropriate choice for the investigated scanner.

Keywords: Acceptance Angle · Total Body J-PET · Sensitivity · Spatial Resolution.

1 Introduction

Positron Emission Tomography (PET) is an advanced diagnostic method that allows for non-invasive imaging of ongoing physiological processes in the human body. Detection of malignant lesions, is one of the main clinical tasks of PET scan. The fact that the principle of operation of positron tomography is at the

molecular level, opens a possibility to detect malignant tissues in very early stages. Furthermore, it is also used to monitor the treatment of patients. For that, the standardized uptake value (SUV) is being considered as an index based on the concentration of the radiopharmaceutical in the formerly detected lesion. Any change of this parameter between successive imaging sessions can be used to assess patient response to therapy [1].

Most of the current clinically available PET scanners have an axial field of view (AFOV) of 15-26 cm [2]. In order to image the entire body the iterative or continuous bed movement is applied allowing for part-by-part imaging of human and finally, after combination, for the whole body image. However, this method has a very low sensitivity of $\sim 1\%$ which comes from the fact, that at any one time most of the body is outside the FOV and only a small fraction of emitted photons can be detected due to isotropic radiation [2, 3]. In order to address those factors the Total Body PET concept, characterised by coverage of the entire human with the detector rings has been proposed. There are currently at least four groups/projects concerning such systems: the UC Davis EXPLORER Consortium [4, 5], the Ghent University “PET 2020” [6], the Siemens Healthineers “Biograph Vision Quadra” [7] and the J-PET Collaboration [8–11] from the Jagiellonian University in Cracow, Poland. The benefits of TB PETs are not limited to just single bed position imaging or no need for motion correction but also, thanks to a huge gain in sensitivity, the possibility of an increase in the signal-to-noise ratio, reduction in time of the scan, or decrements in activity dose according to the ALARA principle [12]. Moreover, when it comes to lesion detectability, they can be used to detect even sub-centimeter specimens [2, 3].

Nevertheless, long AFOV creates new challenges in image reconstruction and event selection. While the possibility of detection of additional LORs contributes positively to the sensitivity of the tomograph, it has an unfavorable influence on spatial resolution. Moreover, strong attenuation of oblique LORs in the body results in the increase of unwanted scattered coincidences and enlarges the parallax error. This forces to determine a new parameter such as an acceptance angle as a cut over all registered LORs. Acceptance angle is a maximum azimuthal angle for which the line of responses are still taken into image reconstruction (see Figure 1) [13]. For different geometries of PET scanners, it can be defined either as an angle or as a ring difference. However, such an acceptance cut is creating a tradeoff between two main parameters of PET scanners: sensitivity and spatial resolution.

The presented study is focused on the Total Body system proposed by the Jagiellonian PET Collaboration. The J-PET Collaboration presents an innovative approach to the design of PET systems. In oppose to the common tomographs equipped with inorganic, radially arranged scintillator crystals, J-PET uses axially arranged plastic scintillator strips read out on both ends with silicon photomultipliers. With a geometry which allows to significantly reduce the amount of needed electronics and smaller number of scintillators, J-PET strives to be the cost-effective competitor for PET imaging [9, 11, 14–19].

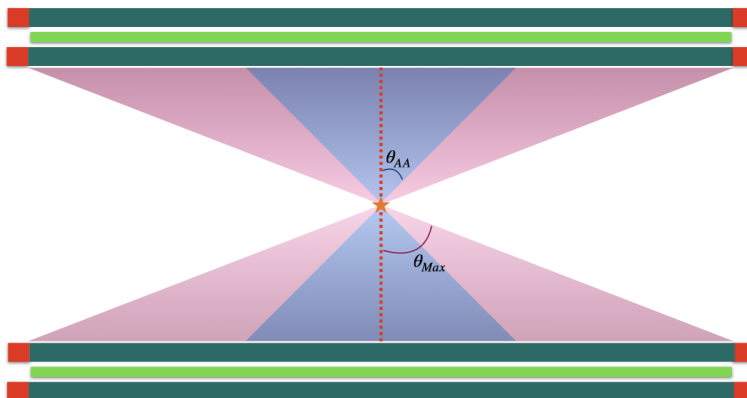


Fig. 1: Schematic cross section view of TB J-PET scanner simulated in this work. TB J-PET detector is composed of long strips of plastic scintillator (dark green) read out at two ends by photomultipliers (red). Two layers of scintillator strips are interleaved with the WLS layer (light green). It has 2 meter long axial field of view and 78.6 centimeters of inner diameter. The structure of the detector is described more detailed in Figure 2. The pink cone (wider one) created by the maximal angle θ_{Max} which for this geometry is equal to 69° , contains all possible LORs originating from the centrally located point source (marked as a star) which can be detected by the tomograph. The θ_{AA} denotes an exemplary acceptance angle for which only the LORs located within the blue cone (narrower one) are taken into account during further analysis.

The effect of the oblique LORs has already been researched for the previously investigated Total Body J-PET system (TB J-PET) composed of a single layer with 384 plastic scintillators. The study was performed using the NEMA IEC-Body phantom based on the Filtered Back Projection (FBP) algorithm with STIR package [20]. The presented here simulation-based study was carried out in order to determine the proper acceptance angle for a newly proposed Total Body J-PET scanner with a multi-layer arrangement of plastic scintillators. Instead of the FBP, it was based on the Ordered Subset Expectation Maximization (OSEM) iterative image reconstruction algorithm. Recently, the iterative image reconstruction-based algorithms have been widely developed due to their superior performance in comparison with the traditionally used ones. They are significantly reducing noise and improving the image quality. OSEM is one of the main examples of such widely used iterative methods, which allows for a more precise model of PET acquisition procedure [21].

2 Methods

This study concerns one of the proposed and investigated by the J-PET Collaboration Total Body (TB) systems. The TB J-PET scanner has been simulated

using Geant4 Application for Tomographic Emission (GATE) software [22–24]. GATE is a validated toolkit based on Monte Carlo simulations developed to research nuclear medicine systems. Considered tomograph consists of 24 panels which are parallel to the central axis of the tomograph (see Figure 2). Each

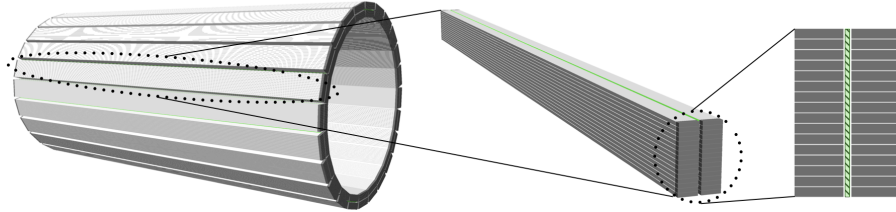


Fig. 2: (Left) Visualization of the Total Body J-PET scanner which consists of 24 axially arranged panels. (Middle) The panel is composed of 2 modules, each with 16 EJ230 plastic scintillation strips. (Right) In order to enhance axial resolution, modules are separated by an array of perpendicularly arranged WLS strips marked with green color (hash line pattern).

panel is made from 2 modules separated by an array of wavelength-shifting (WLS) strips [25]. The module consists of 16 EJ230 “Eljen Technology” plastic scintillation strips with a dimension of $6 \times 30 \times 2000 \text{ mm}^3$ located next to each other with 0.5 mm intervals between them. Each strip is coupled on both ends with a silicon photomultipliers [11].

For this study, two types of simulations have been performed using described geometry. The first simulation type included a 183 cm long linear source with a diameter of 1 mm and 1 MBq of total activity. In order to evaluate the contribution of phantom scatter coincidence events in all registered types of events, the study was also carried out with a centrally located, cylindrical phantom. The water filled phantom with 10 cm radius and 183 cm length³ was simulated once without background activity and once with background activity of 10:1 target background ratio (TBR) to imitate the real, non-uniform activity distribution in the human body. The second group consisted of a situated in the center 1 MBq point like source placed inside a 20 cm long cylindrical air phantom with 20 cm radius and with 10:1 TBR. The hit-based result of the GATE simulation was analyzed using GOJA software. Gate Output J-PET Analyzer (GOJA) is a developed by J-PET Collaboration specialized software used for analyzing and construction of coincidence events based on the GATE hits output for J-PET-like tomographs [26]. For the case of this study, the time window has been set to 5 ns, while lower energy threshold to 200 keV in order to minimize the number

³ The length of the source and phantom was set to 183 cm which represents the average man height in the tallest country in the world [2]

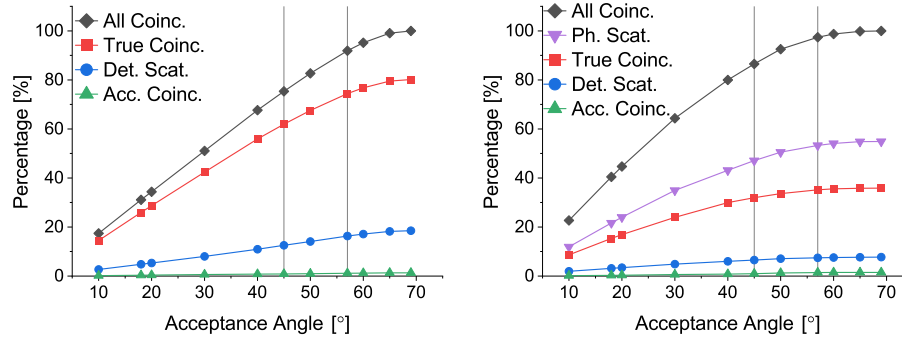
of detector scatter coincidences [27]. Due to the innovative geometric design of Total Body J-PET, most of the commonly used for image reconstruction softwares are not valid for the multi-layer PET scanner. One of the exceptions from that, is the Quantitative Emission Tomography Iterative Reconstruction (QETIR) software developed by Medisip group [28], which was chosen for the case of this study. Alongside image reconstruction application based on the OSEM algorithm, QETIR is also able to generate all of the needed requirements like sensitivity map and attenuation map. The generation of the sensitivity map was done with $3.125 \times 3.125 \times 3.125 \text{ mm}^3$ voxel size and the reconstruction performed by 4 iterations with 25 subsets in each of them.

3 Results

In order to estimate a proper Acceptance Angle (from now on referred to as θ_{AA} angle) for the investigated Total Body J-PET scanner, four types of studies have been done based on the described simulations. Firstly, the effect of various θ_{AA} angles on the percentage share of each type of coincidence events in the total number of registered events (when $\theta_{AA} \equiv \theta_{Max} = 69^\circ$) has been estimated for a group of simulations of a line source (see Figure 3). The range of the tested angles covers the region from 10° to 65° angle. The influence of the 18° angle, which is a maximal achievable angle for traditional clinical PET tomographs was also inspected [29]. However, in this study, we are particularly emphasizing the 45° and 57° acceptance angles, which were already determined for different Total Body PET systems [30, 31].

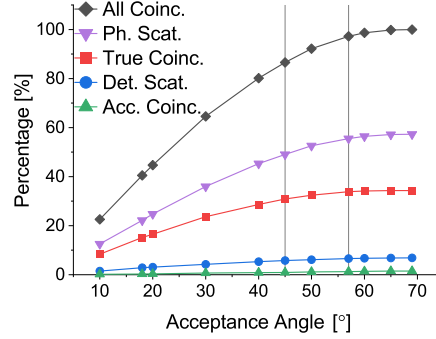
While the number of each type of coincidences increases together with the widening of θ_{AA} angles, this relation is not linear especially for higher angles. Based on the simulation with line source (see Figure 3a) it can be estimated, as anticipated in [13], that there is no significant increment in the number of each type of registered events for acceptance angle larger than 57° . In case of having a phantom (see Figures 3b & 3c) there is an addition of new type of coincidences which is a Phantom Scatter. For angles higher than 45° there is no meaningful change (only increase from 31.9% to 35.9% in case of simulation with background activity and from 30.9% to 34.3% for simulation without background activity) in the percentage share of True Coincidences. However, the 45° angle gives 14% reduction of undesirable Phantom Scatters, which is almost 5 times better than for 57° angle.

The second study concerned the determination of the influence of θ_{AA} angle on the sensitivity of TB J-PET tomograph. Sensitivity is one of the main parameters taken into account in lesion detectability of PET scanners [3]. Two parameters: Total Sensitivity and Sensitivity @ Center, were determined for each acceptance angle. The Total Sensitivity was calculated as a mean of sensitivity of every slice, while the sensitivity of a slice was estimated as the rate of registered events divided by the fraction of activity per slice. The Sensitivity @ Center is the sensitivity of the central slice (at 0 cm). Moreover, the same calculation was performed also for only True Coincidences with a change in the definition of



(a) Fraction of coincidences as a function of the acceptance angle determined based on the simulation of 1 MBq line source.

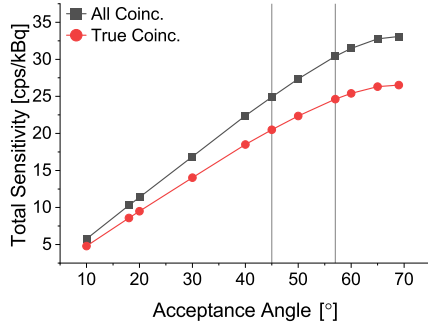
(b) Fraction of coincidences as a function of the acceptance angle determined based on the simulation of 1 MBq line source and 183 cm long water phantom with background activity.



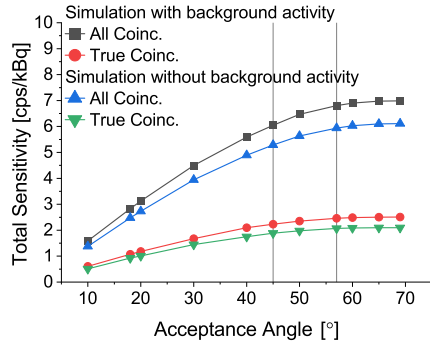
(c) Fraction of coincidences as a function of the acceptance angle determined based on the simulation of 1 MBq line source and 183 cm long water phantom without background activity.

Fig. 3: Plots represent the percentage share of all and each type of coincidence events for a given acceptance angle in the total number of registered events for 69° acceptance angle (which is the maximal possible angle which LOR can have in presented geometry). Abbreviations used in the legend: ‘All Coinc.’, ‘Ph. Scat.’, ‘True Coinc.’, ‘Det. Scat.’ and ‘Acc. Coinc.’ denote All Coincidences, Phantom Scatter, True Coincidences, Detector Scatter and Accidental Coincidences, respectively. Especially researched 45° and 57° angles are marked with vertical lines.

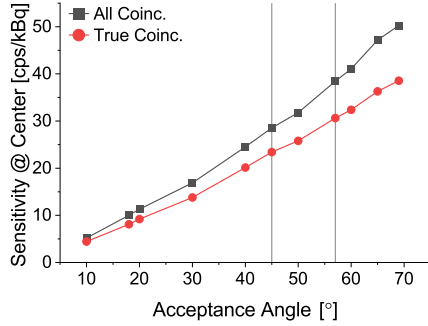
sensitivity in each slice from the rate of registered events to the rate of registered True Coincidence events. Figures 4a and 4b present the values of the first sensitivity parameter as a function of θ_{AA} from the simulation of line source without



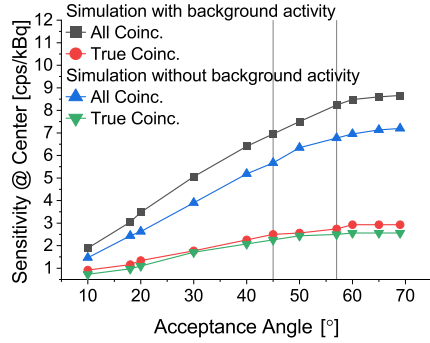
(a) Dependence of Total Sensitivity on acceptance angle determined based on the simulation of 1MBq line source.



(b) Dependence of Total Sensitivity on acceptance angle determined based on the simulation of 1 MBq line source and 183 cm long water phantom.



(c) Dependence of Sensitivity @ Center on acceptance angle determined based on the simulation of 1MBq line source.



(d) Dependence of Sensitivity @ Center on acceptance angle determined based on the simulation of 1 MBq line source and 183 cm long water phantom.

Fig. 4: Results of Total Sensitivity and Sensitivity @ Center obtained with different acceptance angles for true (all) coincidences. The Total Sensitivity was calculated as a sum of sensitivities of each slice divided by the number of them, where the sensitivity of each slice is described as the rate of registered events resulting in true coincidences (any type of coincidences) divided by according fraction of activity. The Sensitivity @ Center is equal to the sensitivity of the central slice. Especially researched 45° and 57° angles are marked with vertical lines.

and with phantom, respectively. The results of the latter parameter are shown in the figures 4c and 4d. Based on the Figure 4a, the acceptance angle has a huge impact on the Total Sensitivity. Considered 45° and 57° angles correspond to losses of ~24.3% (~22.7%) and ~7.7% (~7.1%) respectively for All (True) types of coincidence events. However, for the more realistic simulation with a phantom

with warm background (see Figure 4b), the influence of θ_{AA} angle is smaller and the 45° angle is reducing the Total Sensitivity only by $\sim 13.4\%$ in case of All events and $\sim 11.2\%$ in case of True Coincidences. The corresponding Sensitivity @ Center (see Figure 4d) is equal to 6.95 cps/kBq for All and 2.50 cps/kBq for True events, which is accordingly $\sim 80.3\%$ and $\sim 85.3\%$ of the maximal possible central sensitivity.

Furthermore, the effect of acceptance angle on a scatter fraction was investigated. The scatter fraction of the PET scanner quantifies the sensitivity of the detector to scattered radiation [32]. It was estimated as a ratio of the sum of Phantom and Detector Scatter to the number of All Coincidences. The relation between scatter fraction and θ_{AA} angle determined based on the simulations with 1 MBq line source and water phantom is presented in Figure 5. In both cases the maximum minimization to 10° of the acceptance angle is reducing this parameter only by $\sim 2\%$. However, the noticeable growing trend with wider θ_{AA} suggests, that in case of higher activities the acceptance angle factor can contribute positively to the scatter fraction reduction.

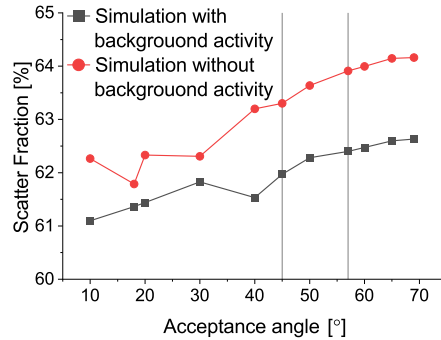


Fig. 5: The plot represents the scatter fraction as a function of the acceptance angle determined based on the simulations of 1 MBq line source and 183 cm long water phantom. Especially researched 45° and 57° angles are marked with vertical lines.

Spatial resolution is one of the most important characteristics of PET scanners, which determines the possible size of detectable lesions [32–34]. One of the classic approaches to investigate the quality of spatial resolution utilizes a Point Spread Function (PSF). PSF is defined as a full width at half maximum of the either transverse or axial one-dimensional projection of the slice of reconstructed image, which contains the radioactive source. In order to estimate the impact of the acceptance angle on the spatial resolution of Total Body J-PET, a point like source has been simulated inside a cylindrical air phantom with 10:1 target background ratio. Figure 6a presents values of both PSF parameters for 6 different acceptance angles, calculated based on the first iteration with 25 subsets

of image reconstruction. The results show that increase of θ_{AA} has much worse influence on the axial PSF than on transverse PSF. In case of the latter, one can even observe an improvement of resolution for 57° in oppose to 45° angle. However, the effect of number of iterations in image reconstruction on the transverse resolution (see Figure 6b) turns out to not only improve the results but also reverse the ratio between PSF for 45° and 57° angle. Nonetheless, the percentage difference between each calculated point for transverse PSF is much smaller and even this improvement is negligible in comparison to the deterioration in the axial resolution. Moreover, Figure 6c shows that the influence of iterations number on the axial resolution is almost negligible for both angles. In case of the third and fourth iteration for which the ratio in transverse PSF is reversed, the 45° acceptance angle is almost 29% better than 57° in terms of axial resolution and results in axial PSF equal to 4.80(11) mm.

4 Conclusions

The determination of the proper acceptance angle is a mandatory requirement to maximize the performance of Total Body PET systems. The aim of this study was to estimate such optimal angle for the proposed and investigated by the J-PET Collaboration Total Body PET tomograph, based on the simulations performed using GATE software. The presented results show that 45° acceptance angle gives almost 5 times better reduction of undesirable Phantom Scatters than 57° angle. In case of the Total Sensitivity of investigated scanner, the same angle gives a $\sim 13.4\%$ ($\sim 11.2\%$) loss of maximal possible Total Sensitivity for All Coincidences (True Coincidences). No significant difference in the level of scatter fraction was observed. For both 45° and 57° angles it was estimated to $\sim 62.0\%$ ($\sim 63.3\%$) and $\sim 62.4\%$ ($\sim 63.9\%$), respectively for simulation with (without) background activity. However, different θ_{AA} angles have a major influence on the spatial resolution, especially on axial PSF. Discussed local improvement in transverse resolution for 57° angle in oppose to 45° disappears with higher numbers of iterations in image reconstruction, while there is no meaningful change in axial resolution. Based on provided evidence, the 45° acceptance angle seems to be an optimal choice for the Total Body J-PET tomograph.

5 Acknowledgment

This work was supported by Foundation for Polish Science through TEAM POIR.04.04. 00-00-4204/17, the National Science Centre, Poland (NCN) through grant No. 2019/35/B/ST2/03562 and grant PRELUDIUM 19, agreement No. UMO-2020/37/N/NZ7/04106.

The publication also has been supported by a grant from the SciMat Priority Research Area under the Strategic Programme Excellence Initiative at the Jagiellonian University.

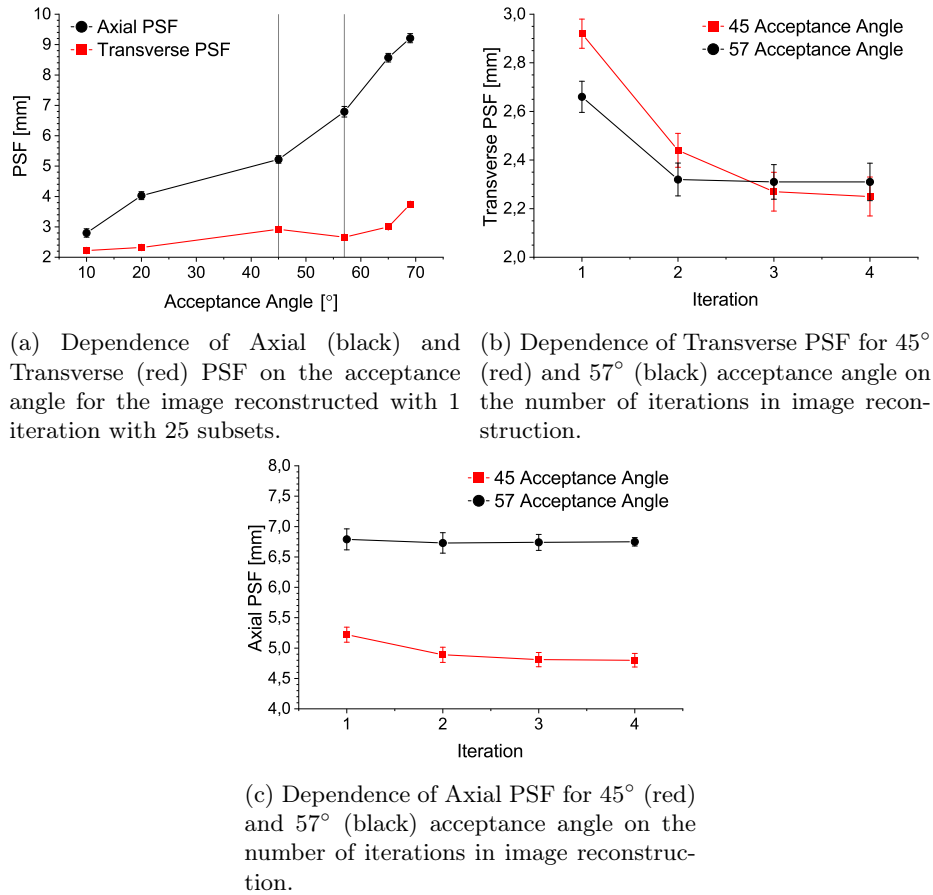


Fig. 6: Plots represent study of the effect of acceptance angle and image reconstruction iterations number on the spatial resolution.

References

- Schaefferkoetter, J., Townsend, D.: A human-trained numerical observer model for PET lesion detection tasks. In: Editor, F., Editor, S. (eds.) IEEE Nuclear Science Symposium and Medical Imaging CONFERENCE 2015, vol. 9999, pp. 1-3. San Diego, C (2015). <https://doi.org/10.1109/NSSMIC.2015.7582063>.
- Vandenberghe S., Moskal P., Karp, J.: State of the art in total body PET. *EJNMMI* **7**(35), (2020).
- Cherry, S.: Total-Body PET: Maximizing Sensitivity to Create New Opportunities for Clinical Research and Patient Care. *J. Nucl. Med.* **59**(1), 3–12 (2018)
- uEXPLORER Homepage, <http://www.explorer.ucdavis.edu>. Last accessed 13 March 2021.
- Badawi, R., Shi, H., Hu, P., et al.: First Human Imaging Studies with the EXPLORER Total-Body PET Scanner. *J. Nucl. Med.* **60**(3), 299–303, (2019).

6. Vandenberghe, S., Geagan, M., Efthimiou, N.: PET2020 HRS: Maximization of sensitivity and resolution using axial extension and patient adaptive rings in a high resolution long axial FOV scanner. pp. 274–274. EUROPEAN JOURNAL OF NUCLEAR MEDICINE AND MOLECULAR IMAGING, 46, (2019).
7. Siemens Healthineers Homepage, <http://www.siemens-healthineers.com/molecular-imaging/pet-ct/biograph-vision-quadra>. Last accessed 13 March 2021
8. J-PET Homepage, <http://www.koza.if.uj.edu.pl/pet/>. Last accessed 13 March 2021.
9. Moskal, P., Stępień, E.: Prospects and Clinical Perspectives of Total-Body PET Imaging Using Plastic Scintillators. PET Clinics **15**(4), 439–452, (2020).
10. Moskal, P., Jasińska, B., Stępień, E.: Positronium in medicine and biology. Nature Reviews Physics volume, **1**, 527–529, (2019).
11. Moskal, P., Rundel, O., Alfs, D., et al.: Time resolution of the plastic scintillator strips with matrix photomultiplier readout for J-PET tomograph. Phys Med Biol **61**(5), 2025–2047 (2016)
12. Karakatsanis, N., Fokou, E., Tsoumpas, C.: Dosage optimization in positron emission tomography: state-of-the-art methods and future prospects. Am J Nucl Med Mol Imaging **5**(5), 527–547 (2015).
13. Efthimiou, N.: New Challenges for PET Image Reconstruction for Total-Body Imaging. PET Clin **15**(4), 453–461 (2020)
14. Moskal, P., Niedźwiecki, Sz., Bednarski, T., et al.: Test of a single module of the J-PET scanner based on plastic scintillators. Nucl. Instr. and Meth. A. **764**, 317–321 (2014).
15. Moskal, P., Kisielewska, D., et al.: Feasibility study of the positronium imaging with the J-PET tomograph. Phys. Med. Biol. **64** (2019) 055017
16. Moskal, P., Kisielewska, D., et al.: Performance assessment of the 2 γ positronium imaging with the total-body PET scanners. EJNMMI Phys. **7** (2020) 44
17. Sharma, S., Chhokar, J., et al.: Estimating relationship between the Time Over Threshold and energy loss by photons in plastic scintillators used in the J-PET scanner. EJNMMI Phys. **7** (2020) 39
18. Moskal, P., Krawczyk, N., Hiesmayr, B. C., et al.: Feasibility studies of the polarization of photons beyond the optical wavelength regime with the J-PET detector. Eur Phys J C **78**(11), 970–980 (2018)
19. Moskal, P., Salabura, P., Silarski, M., et al.: Novel Detector Systems for the Positron Emission Tomography. Bio-Algorithms and Med-Systems **7**(2), 73–78 (2011)
20. Kopka, P., Klimaszewski, K.: Reconstruction of the NEAM IEX Body phantom from J-PET Total-Body scanner simulation using STIR. Acta Phys. Pol. B 51, Poland, 357–360 (2020)
21. Zhu Y. M.: Ordered subset expectation maximization algorithm for positron emission tomographic image reconstruction using belief kernels. Journal of medical imaging (Bellingham, Wash.) **5**(4), (2018)
22. Jan, S., Santin, G., Strul, D., et al.: GATE: a simulation toolkit for PET and SPECT. Phys Med Biol **49**(19), 4543–4561 (2004)
23. Santin, J., Benoit, D., Becheva, E., et al.: GATE V6: a major enhancement of the GATE simulation platform enabling modelling of CT and radiotherapy. Phys Med Biol **56**(4), 881–901 (2016)
24. Sarrut, D., Bardiès, M., Bousson, N., et al.: A review of the use and potential of the GATE Monte Carlo simulation code for radiation therapy and dosimetry applications. Med Phys **41**(6), (2014)

25. Smyrski, J., Alfs, D., Bednarski, T., et al.: Measurement of gamma quantum interaction point in plastic scintillator with WLS strips. *Nuclear Instruments and Methods in Physics Research A* **851**(5), 39–42 (2017)
26. Dadgar, M. Kowalski, P.: GATE Simulation Study of the 24-module J-PET Scanner: Data Analysis and Image Reconstruction, pp. 309–320. *Acta Phys. Pol. B* 51, Poland, (2020)
27. Kowalski, P., Wiślicki, W., Raczyński, L., et al.: Scatter fraction of the J-PET tomography scanner. *Acta Phys. Pol. B* **47**(2), 549–560 (2016)
28. Medisip Homepage, <https://www.ugent.be/ea/ibitech/en/research/medisip>. Last accessed 13 March 2021.
29. Siemens Homepage, <https://www.siemens-healthineers.com/molecular-imaging/pet-ct/biograph-vision>. Last accessed 13 March 2021.
30. Cherry, S. et al.: Abstracts of the Total Body PET conference 2018, pp. 1–2. EJNMMI, Ghent, Belgium (2018)
31. Zhang, X., Xie, Z., Berg, E., et al.: Total-Body Dynamic Reconstruction and Parametric Imaging on the uEXPLORER. *Journal of Nuclear Medicine* **61**(2), 285–291 (2019)
32. Kowalski, P., Wiślicki W., Shopa, R., et al.: Estimating the NEMA characteristics of the J-PET tomograph using the GATE package. *Phys. Med. Biol.* **63**(16), 99–110 (2018)
33. NEMA Homepage, <https://www.nema.org/standards/view/Performance-Measurements-of-Positron-Emission-Tomographs>
34. Pawlik-Niedźwiecka, M., Niedźwiecki, S., Alfs, D., et al.: Preliminary Studies of J-PET Detector Spatial Resolution. *Acta Phys. Pol. A* **132**(5), 1645–1648 (2017)